ChemPhotoChem

Chemistry Europe
European Chemical Societies Publishing
ChemPhotoChem

RESEARCH ARTICLE OPEN ACCESS

Thermally Activated Delayed Fluorescence Sensitization of Bis(phenylethynyl)benzenes for Visible-to-UV Upconversion

Davide Lardani[1] | Alessandra Ronchi[2] | Xueqian Hu[1] | Angelo Monguzzi[2] | Christoph Weder[1]

[1]Adolphe Merkle Institute, University of Fribourg, Fribourg, Switzerland | [2]Department of Materials Science, University of Milano-Bicocca, Milan, Italy

Correspondence: Angelo Monguzzi (angelo.monguzzi@unimib.it) | Christoph Weder (christoph.weder@unifr.ch)

Received: 11 October 2025 | **Revised:** 3 December 2025 | **Accepted:** 8 December 2025

Keywords: heavy-metal-free sensitizers | organic annihilators | thermally activated delayed fluorescence | triplet–triplet energy transfers | UV photons

ABSTRACT

Sensitized triplet–triplet annihilation can be utilized to upconvert low-intensity visible (Vis) light into ultraviolet (UV) light, making it useful for applications powered by short-wavelength sunlight. However, dye systems for this wavelength range are limited. Here, we report that Vis-to-UV upconversion (UC) is achieved with dye pairs that include the thermally activated delayed fluorescence (TADF) luminophores 2,3,5,6-tetrakis(carbazol-9-yl)benzonitrile (4CzBN) or 2,4,5,6-tetrakis(9H-carbazol-9-yl) isophthalonitrile (4CzIPN) as sensitizer and bis(phenylethynyl)benzene (BPEB) or an alkoxylated BPEB derivative as emitter. The photophysical characterization of degassed toluene solutions of the four possible combinations of these dyes reveals efficient triplet energy transfer efficiencies exceeding 80%, upconverted UV emission centered at ca. 380 nm with an anti-Stokes shift of up to 0.64 eV from the blue range of the optical spectrum, excitation threshold intensities as low as ca. 25 mW·cm^{-2}, and UC quantum yields up to 4.5%, depending on the dye combination. These results establish pairs of TADF sensitizers and BPEB emitters as viable candidates for Vis-to-UV (UC), broadening the molecular design space for next-generation photonic and solar-powered UV applications.

1 | Introduction

Harnessing solar energy to power ultraviolet (UV) light-driven chemical transformations, such as water disinfection [1], photopolymerization [2, 3], and UV-induced catalysis [4, 5], is an attractive strategy for increasing the sustainability of such processes. However, the limited UV content of terrestrial sunlight, accounting for less than 10% of the overall spectrum, remains a fundamental bottleneck for direct solar utilization in such applications [6]. To address this limitation, researchers have explored photon upconversion (UC) mechanisms that convert low-energy visible (Vis) light into higher-energy UV photons [7–9]. Among the different strategies to achieve UC, sensitized triplet–triplet annihilation (sTTA) has emerged as a particularly promising approach. This process enables UC under low-intensity, noncoherent excitation conditions such as sunlight [10, 11]. In sTTA-UC, a visible-light-absorbing sensitizer undergoes intersystem crossing (ISC) and its triplet state is populated, followed by Dexter-type triplet energy transfer (ET) to an annihilator/emitter molecule. Collisions between two emitter triplets may result in triplet–triplet annihilation (TTA), generating an emissive singlet excited state and ultimately UV photon emission (Figure 1A).

The success of this mechanism critically depends on the triplet energetics and excited-state dynamics of both the sensitizer and the emitter [12–14]. Historically, the most efficient TTA-UC systems have relied on organometallic sensitizers containing heavy atoms, such as iridium, palladium, or platinum complexes, which achieve high intersystem crossing (ISC) rates through spin–orbit coupling [15, 16]. While highly effective, these sensitizers suffer

Davide Lardani, Alessandra Ronchi contributed equally to this work.

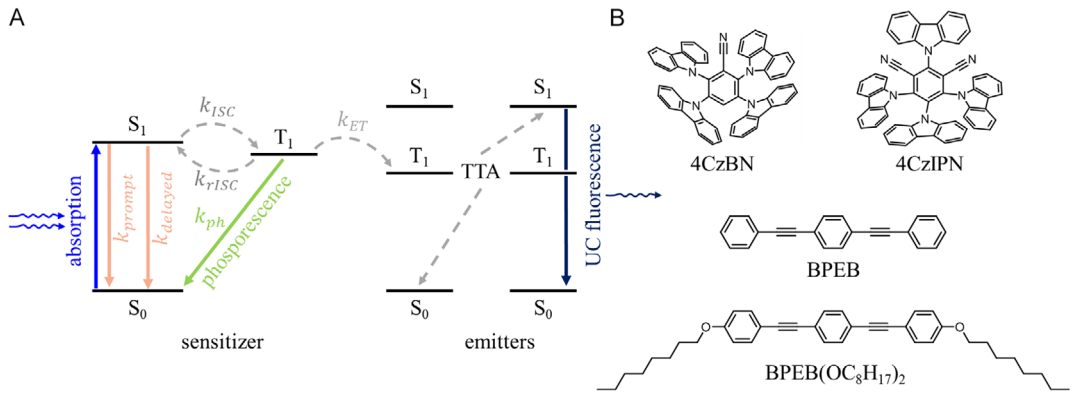

FIGURE 1 | (A) Jablonski diagram outlining the key photophysical events and relative kinetic constants (k) involved in the TTA-UC mechanism. Nonradiative processes, including intersystem crossing (ISC), reverse intersystem crossing (rISC), Dexter-type energy transfer (ET), and triplet–triplet annihilation (TTA), are represented with dashed arrows. The singlet ground state (S_0), the first excited singlet state (S_1), and the first excited triplet state (T_1) are depicted as energy levels. (B) Chemical structure of the TADF sensitizers 4CzBN and 4CzIPN and the UV emitters BPEB and BPEB(OC_8H_{17})$_2$.

from drawbacks including high cost, limited availability, potential toxicity, and narrow absorption profiles that restrict their ability to harvest a broad portion of the sunlight [17]. To overcome these limitations, thermally activated delayed fluorescence (TADF) molecules have emerged as attractive metal-free alternatives. Originally developed for organic light-emitting diodes (OLEDs), TADF compounds possess small singlet–triplet energy gaps and long-lived excited states, enabling efficient ISC and reverse ISC (rISC) through thermal activation [18–21]. The potential advantages of TADF sensitizers include their broad and strong visible absorption, structural modularity, and absence of toxic metals. However, the main feature that makes TADFs efficient in OLEDs, the rISC process, can be detrimental for TTA-UC, as it depletes the population of sensitizer triplets that are meant to be transferred to the annihilator [22, 23]. Nevertheless, when appropriately designed, TADF compounds can act as effective triplet sensitizers, provided their ISC/rISC dynamics and energy levels are suitably tuned relative to the emitter [24–27]. Several groups have already demonstrated Vis-to-UV TTA-UC using TADF-based sensitizers, establishing this approach as a viable option [28, 29]. Yanai and coworkers, for example, highlighted the importance of energy level alignment between the TADF donor 4CzIPN and high-triplet-energy acceptors such as *p*-terphenyl and *p*-quaterphenyl. Their optimized pairings achieved anti-Stokes shifts up to 0.83 eV and UC quantum yields as high as 3.9%, with emission extending below 350 nm [30]. To overcome the common limitations associated with triplet diffusion and rISC, Peng et al. developed a series of heavy-atom-free bichromophoric TADF photosensitizers incorporating covalently tethered acceptors [31]. Their intramolecular ET design significantly suppressed rISC, enabling high triplet yields and prolonged triplet lifetimes, which both contributed to achieving efficient TTA-UC under low excitation conditions, even in solid-state polymer films. Baldo and coworkers demonstrated the feasibility of solid-state UC using a bilayer architecture comprising the TADF dye 4CzTPN-Ph and 9,10-diphenylanthracene (DPA). While the overall quantum yields were modest and the emission was in the blue and not the UV regime, this proof-of-concept highlighted the potential of metal-free UC in condensed phases [32]. Expanding the functional scope of TTA-UC, Han and collaborators developed a chiral UC platform based on a TADF sensitizer and a chiral annihilator embedded in a chiral nematic liquid crystalline material [33]. Their system enabled circularly polarized UV emission for enantioselective photopolymerization, exemplifying how TADF-based UC can be tailored for advanced optical applications. Kerzig and coworkers demonstrated a purely organic Vis-to-UV UC system featuring a biphenyl-based annihilator with a singlet-excited-state energy above 4.0 eV. Paired with 4CzIPN, the system delivered a record anti-Stokes shift of 1.17 eV, extending the usable energy window for demanding photochemical processes [34]. In a performance benchmark, Albinsson, Moth–Poulsen, and colleagues reported a TTA-UC system combining 4CzBN with various high-energy annihilators, including PPD, TP, 2PI, PPO, PPF, and TIPS-Naph. They achieved an internal UC quantum yield of 16.8%, approaching the spin-statistical limit, and underscoring the potential of carefully engineered organic sensitizers for highly efficient UV UC [35]. Lee and coworkers presented an all-organic system pairing 4CzIPN with pyrene, capable of efficient UC under air-saturated conditions. Their approach leveraged oleic acid to quench singlet oxygen and demonstrated higher UC efficiency than classical biacetyl/PPO systems [36]. Finally, Chen and collaborators developed a bichromophoric sensitizer by tethering a pyrene acceptor to a 4CzPN core. This motif enabled fast, irreversible intramolecular ET and suppressed rISC, facilitating UC even in diffusion-limited or low-concentration environments such as polymer matrices [27]. Collectively, these studies illustrate the growing functional and structural diversity of TADF-based TTA-UC platforms, including solution-based, solid-state, and chiral systems. While significant progress has been made, especially with respect to quantum yield and spectral range, the development of robust, photostable UV-emitting annihilators remains a key challenge for the future. We recently introduced a new family of UV-emitting annihilators based on a bis(phenylethynyl)benzene (BPEB) core, which are easily synthetically accessible, photostable, and structurally tunable [37]. In combination with the iridium complex Ir(ppy)$_3$ in degassed toluene, these emitters enable efficient Vis-to-UV UC with maximum emission around ca. 380 nm under low excitation power density [38]. Considering the above-discussed advantages and examples, we sought to investigate the potential of TADF sensitizers, specifically 4CzBN and 4CzIPN, as metal-free alternatives in combination with such emitters. We pair these sensitizers with BPEB or its alkoxylated

derivative BPEB(OC_8H_{17})$_2$ (Figure 1B) and study their interactions and UC performance.

2 | Results and Discussion

2.1 | Energy Transfer Measurements

To evaluate the efficiency of energy transfer (Φ_{ET}) from the sensitizers to the emitter triplets, we performed steady-state and time-resolved photoluminescence (PL) measurements in degassed toluene solutions. As previously demonstrated by Olesund and coworkers [35], when the sensitizer's singlet-triplet energy difference $\Delta_{S-T} < 0.1$ eV, Φ_{ET} can be expressed by the ratio of the total sensitizer emission intensity (prompt + thermally activated delayed emission) in the presence (I_{ph}) and absence (I^0_{ph}) of any emitter or by the ratio of the corresponding delayed fluorescence lifetimes according to Equation (1) [39]:

$$\Phi_{ET} = 1 - \frac{I_{ph}}{I^0_{ph}} = \Phi_{isc}\left(1 - \frac{\tau_d}{\tau^0_d}\right) \quad (1)$$

By contrast, when $\Delta_{S-T} > 0.1$ eV, a more reliable Φ_{ET} estimation results from the analysis of the delayed fluorescence lifetimes [35]:

$$\Phi_{ET} = \Phi_{isc}\left(1 - \frac{\tau_d}{\tau^0_d}\right) \quad (2)$$

To apply Equation (2), we utilized Φ_{isc} values from the literature ($\Phi_{isc} = 0.89$ for 4CzBN and $\Phi_{isc} = 0.73$ for 4CzIPN) [35, 40]. We first compared I^0_{ph} of a solution of 4CzBN ($c = 5 \times 10^{-4}$ M) with I_{ph} of solutions containing 4CzBN and either BPEB or its alkoxylated derivative BPEB(OC_8H_{17})$_2$ ($c = 5 \times 10^{-3}$ M). All experiments were carried out in degassed toluene. As shown in Figure 2A, the absorption spectra of the mixtures represent superpositions of those of the individual components, while the steady-state emission spectra, recorded under continuous wave (cw) irradiation at 405 nm, show a broad emission peak with a maximum at ca. 450 nm that is characteristic of 4CzBN emission [35].

Upon addition of either emitter, the intensity of the 4CzBN emission band is notably reduced. Because singlet transfer is not a possibility (Figure 1A, Figure 2A), the quenching process must, in both cases, involve triplet–triplet energy transfer. The analysis according to Equation (1) yields a $\Phi_{ET} = 72\%$ for BPEB and $\Phi_{ET} = 68\%$ for BPEB(OC_8H_{17})$_2$. We assume the small difference to be related to experimental error, as intensity-based methods are more susceptible to reabsorption effects and uncertainty in the dyes' concentration. Time-resolved PL experiments (Figure 2B) show that the prompt fluorescence lifetimes of 4CzBN (ca. 1.6 ns, Supporting Figure S2) remain essentially unchanged upon addition of either emitter (Figure S1), supporting the selective quenching of the triplet manifold via ET. Indeed, the data reveal a pronounced reduction of the delayed fluorescence lifetime (τ_d) of 4CzBN in the presence of the emitters. The intrinsic lifetime $\tau_{d,0} = 25.3$ µs of the delayed emission component of the neat 4CzBN (30% of the total emission, Figure S2 and Table S1) decreases to $\tau_{d,BPEB} = 170$ ns for the solution containing BPEB and $\tau_{d,BPEB(OC_8H_{17})_2} = 100$ ns for the solution containing BPEB(OC_8H_{17})$_2$. The data analysis according to Equation (2) affords $\Phi_{ET} = 88\%$ for both pairings, indicating highly efficient triplet–triplet ET regardless of whether the BPEB core is alkoxylated or not. Moreover, the identical Φ_{ET} values derived from lifetime measurements point to comparable Dexter-type coupling and triplet energy alignment between 4CzBN and the two emitters. These results confirm that the alkoxy substitution on the BPEB scaffold does not significantly alter its triplet-accepting properties, as already reported in our previous study [38]. In addition, we also demonstrate that 4CzBN serves as an efficient triplet donor for both BPEB derivatives. The differences between the Φ_{ET} values calculated from Equations (1) and (2) are consistent with a TADF sensitizer with $\Delta_{S-T} > 0.2$ eV, and are accounted for in the evaluation of the system UC efficiency (Experimental Section) [35, 40]. We next evaluated the triplet–triplet Φ_{ET} from 4CzIPN to the BPEBs using the same methods and conditions as detailed above. As shown in Figure 3A, the steady-state PL spectra also reveal significant quenching of the 4CzIPN emission upon addition of either emitter.

The energy transfer efficiencies determined from these data using Equation (1) are $\Phi_{ET} = 66\%$ for BPEB and $\Phi_{ET} = 67\%$ for BPEB(OC_8H_{17})$_2$, respectively. The time-resolved measurements (Figure 3B) reveal very similar Φ_{ET} values of 66% and 68%,

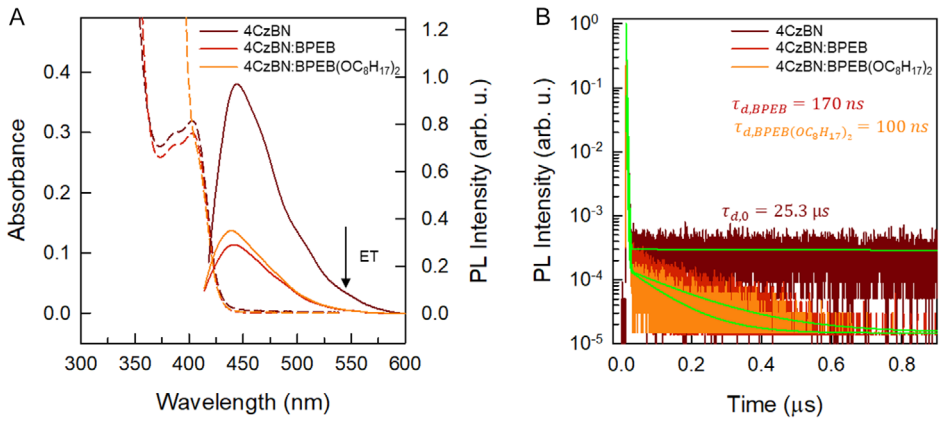

FIGURE 2 | (A) Absorption (dashed lines) and steady-state PL (solid lines) spectra of 4CzBN in the absence (dark red) and presence of BPEB (red) or BPEB(OC_8H_{17})$_2$ (orange) in degassed toluene ($c = 5 \times 10^{-4}$ M for 4CzBN and $c = 5 \times 10^{-3}$ M for BPEB and BPEB(OC_8H_{17})$_2$). (B) Time-resolved PL decay of the same solutions, measured at 450 nm after pulsed excitation at 405 nm, showing quenching of the delayed fluorescence upon addition of BPEB or BPEB(OC_8H_{17})$_2$.

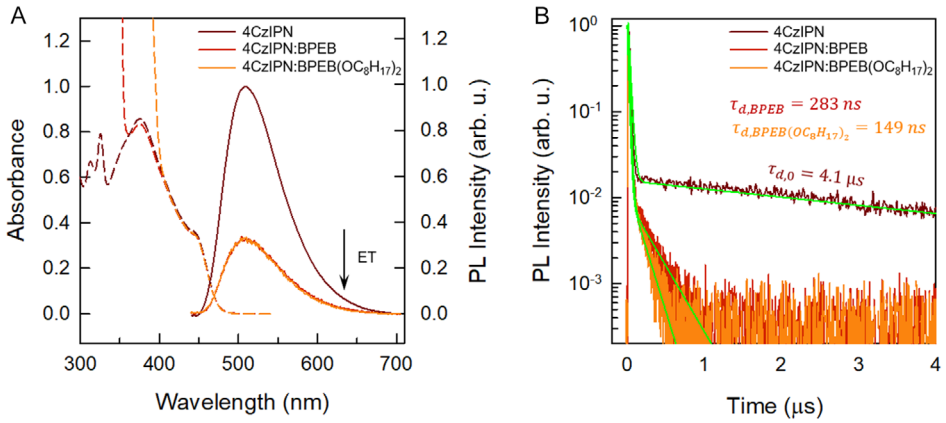

FIGURE 3 | (A) Absorption (dashed lines) and steady-state PL (solid lines) spectra of 4CzIPN in the absence (dark red) and presence of BPEB (red) or BPEB(OC_8H_{17})$_2$ (orange) in degassed toluene ($c = 5 \times 10^{-4}$ M for 4CzIPN and $c = 5 \times 10^{-3}$ M for BPEB and BPEB(OC_8H_{17})$_2$). (B) Time-resolved PL decay of the same solutions measured at 505 nm after pulsed excitation at 405 nm, showing delayed fluorescence quenching upon addition of BPEB or BPEB(OC_8H_{17})$_2$.

respectively, based on a decrease in the lifetime of the 4CzIPN delayed fluorescence component (66% of the total emission, see Figure S4 and Table S2) from $\tau_{d,0} = 4.4$ µs to $\tau_{d,BPEB} = 283$ ns in the presence of BPEB and $\tau_{d,BPEB(OC_8H_{17})_2} = 149$ ns in the case of BPEB(OC_8H_{17})$_2$. The excellent agreement between lifetime-based and intensity-based determinations indicates consistent ET dynamics across both measurement methods, as expected for a TADF sensitizer with $\Delta_{S-T} << 0.1$ eV. Again, the prompt fluorescence lifetimes of 4CzIPN (ca. 15 ns, Figure S4) remain unchanged upon addition of the emitters, confirming that only the triplet manifold is involved in the quenching and supporting the Dexter-type nature of the ET. Compared to the 4CzBN-based systems discussed above, the overall Φ_{ET} values for 4CzIPN are lower (66–68% vs. 88%), indicating that 4CzIPN acts as a less effective triplet donor toward the BPEBs. This difference may arise from its intrinsic triplet state properties, such as faster rISC from T_1 to S_1, which reduces the triplet lifetime from ~25 µs in 4CzBN to ~4 µs for 4CzIPN, and therewith the time available for transfer towards the annihilators [41]. The occurrence of a faster and more efficient rISC for 4CzIPN is reflected by the effective difference observed in the time zero intensity of the TADF emission, which is more than ten times higher than in 4CzBN (Figure 3B and Table S1 and S2). This demonstrates a more efficient population of singlets from triplets, which is consistent with the smaller Δ_{S-T} value.

Subtle differences in triplet energy alignment or Dexter coupling efficiency with the emitters could further partially limit the ET performance, but despite these differences, both BPEB and BPEB(OC_8H_{17})$_2$ effectively quench the 4CzIPN as well as 4CzBN emission, demonstrating successful triplet sensitization and confirming the viability of these dye pairs for metal-free TTA-UC. This is further confirmed by concentration-dependent measurements of Φ_{ET}, which point out similar ET rate constants for the different dye combinations (Figure S5).

2.2 | UC Properties

To assess the TTA-UC performance of the four dye pairs, we evaluated two key figures of merit, namely the UC quantum yield (Φ_{UC}), defined as the number of emitted upconverted photons versus the absorbed ones, and the threshold excitation intensity (I_{th}), which is the excitation intensity at which the TTA yield is 0.5. For this purpose, degassed toluene solutions containing the dyes at the same concentrations used for the energy transfer experiments previously discussed were employed. Figure 4A,C show UC emission spectra of degassed solutions of 4CzBN and BPEB or BPEB(OC_8H_{17})$_2$ excited with a 405 nm cw laser.

In addition to pronounced residual 4CzBN emission at ca. 450 nm, the spectra reveal the characteristic emission bands of the BPEB emitters, centered at ca. 380 nm for 4CzBN:BPEB and ca. 400 nm for 4CzBN:BPEB(OC_8H_{17})$_2$, which become more prominent as the excitation power is increased. Plots of the integrated UC emission intensity against absorbed excitation power (Figure 4B,D) display the expected power dependences, i.e., quadratic relationships at low excitation intensities, characteristic of the TTA mechanism, which convert into linear behaviors at higher power where the UC efficiency is maximized [12, 42]. The intersection of these regimes defines the absorbed power threshold intensity $I_{th,abs}$, which was determined to be ca. 182 mW·cm^{-2} for the 4CzBN:BPEB pair and significantly lower, ca. 25 mW·cm^{-2}, for 4CzBN:BPEB(OC_8H_{17})$_2$. To shed light on this difference, we recorded the UC emission decays under modulated excitation as shown in the insets of Figure 4B,D. These measurements confirm the characteristic TTA dynamics, where the decay rate increases with increasing excitation intensity due to increased triplet population. The time-resolved UC decays can be described by [43, 44]:

$$I_{UC}(t) \sim \left(\frac{1-\Phi_{TTA}}{e^{\frac{t}{\tau_T}} - \Phi_{TTA}}\right)^2 \quad (3)$$

where τ_T is the triplet lifetime of the emitter and Φ_{TTA} is the TTA efficiency at $t = 0$. At low excitation intensities ($\Phi_{TTA} \ll 1$), the decay approximates a monoexponential function, while at higher intensities, the TTA becomes dominant and accelerates the decay dynamics. As expected, Φ_{TTA} increases with the excitation power, transitioning from inefficient annihilation at low triplet densities to nearly complete TTA at higher intensities. Conversely, by fitting the UC decay traces at the lowest excitation intensity

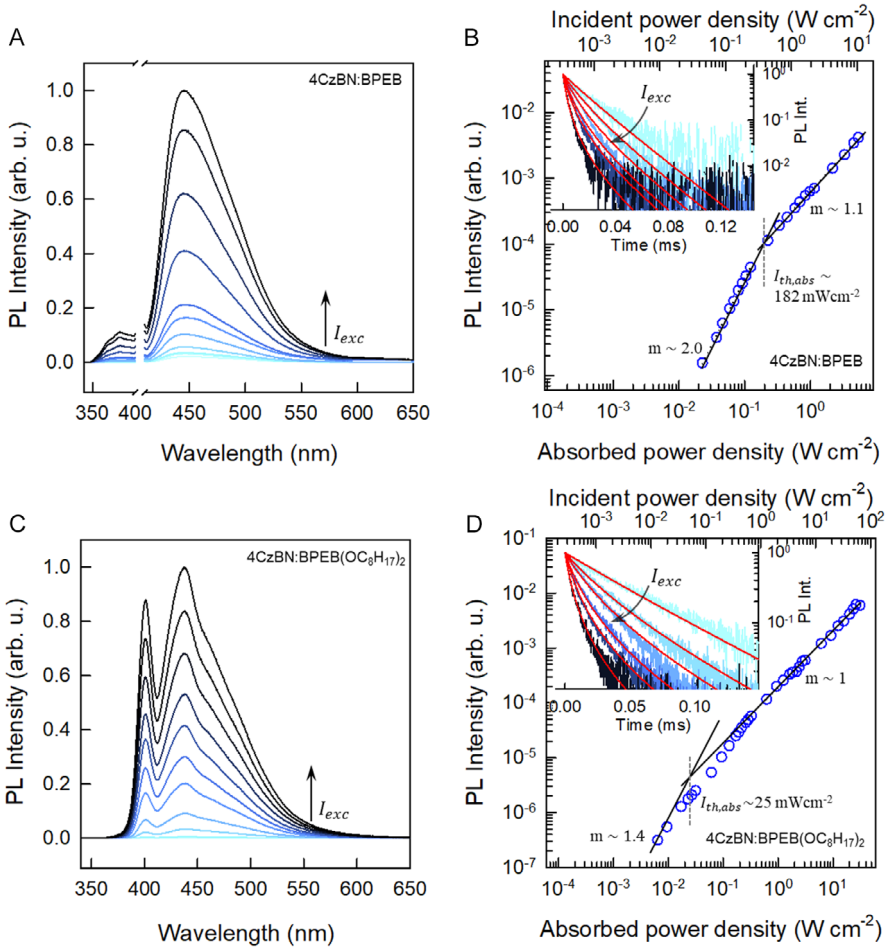

FIGURE 4 | (A,C) Spectra showing the upconverted emission of degassed solutions of 4CzBN and BPEB or BPEB(OC_8H_{17})$_2$ in toluene (c 4CzBN = 5×10^{-4} M; c BPEB/BPEB(OC_8H_{17})$_2$ = 5×10^{-3} M) under cw excitation at 405 nm. The excitation intensity I_{exc} was gradually increased. Aside from the residual 4CzBN emission band with maximum at 450 nm, the spectra show an I_{exc}-dependent increase in emission centered around 380 (A) and 400 nm (C). (B,D) Double-log plots of integrated UC PL intensity versus absorbed power density for 4CzBN:BPEB and 4CzBN:BPEB(OC_8H_{17})$_2$ (blue circles). The solid black lines with slope given by the parameter m reported represent linear fits used to determine the intersection point corresponding to a threshold intensity of ca. 182 (B) and 25 (D) mW·cm^{-2}. The insets show time-resolved UC emission decays recorded at increasing excitation intensities (shaded traces).

with a single exponential model, we estimated the triplet lifetimes of $\tau_T = 39$ μs for 4CzBN:BPEB and $\tau_T = 92$ μs for 4CzBN:BPEB(OC_8H_{17})$_2$. Because the UC threshold value depends quadratically on the annihilator triplet lifetime when using the same type and concentration of sensitizer according to [42]:

$$I_{th} \propto \frac{(k_T)^2}{\Phi_{ET}} \quad (4)$$

where $k_T = [\tau_T]^{-1}$ is the emitter triplet decay rate, the observed disparity in I_{th} must be primarily attributed to the observed differences in the lifetime of the annihilating triplets. For excitation intensities well above the threshold, we measure a maximum UC quantum yield Φ_{UC} = 0.8% for the 4CzBN:BPEB pair, using the residual sensitizer emission as an internal standard in the linear regime ($I_{exc,abs} = 1$ W cm^{-2}) as discussed in Section 4.5. The Φ_{UC} increases to 1.8% for the 4CzBN:BPEB(OC_8H_{17})$_2$ pair, in agreement with the enhanced singlet generation ability of the modified annihilator previously observed [38]. We next evaluated the UC performance of 4CzIPN paired with the annihilators under identical experimental conditions, except that the cw excitation was shifted to 473 nm to match the absorption of 4CzIPN. The UC emission spectra (Figure 5A,C) also feature UC emission centered at ca. 380 nm for BPEB and ca. 400 nm for BPEB(OC_8H_{17})$_2$ in addition to a broad residual sensitizer emission at ca. 510 nm.

Double-logarithmic plots of integrated UC intensity versus the absorbed power density (Figure 5B,D) also reveal, for these pairs, the typical transitions from quadratic to linear regimes, indicative of TTA-dominated behavior. The $I_{th,abs}$, determined from the intersection of linear fits, are ca. 179 mW·cm^{-2} for 4CzIPN:BPEB and ca. 173 mW·cm^{-2} for 4CzIPN:BPEB(OC_8H_{17})$_2$, which is comparable to the value of 4CzBN:BPEB (182 mW·cm^{-2}), but notably higher than that of 4CzBN:BPEB(OC_8H_{17})$_2$ (25 mW·cm^{-2}). Time-resolved UC emission decays (Figure 5B, insets) shed light on this point. Both 4CzIPN-based systems exhibit characteristic TTA decay profiles with excitation-intensity-dependent kinetics. The triplet lifetimes retrieved from mono-exponential fits at the lowest intensities are $\tau_T = 40$ μs for 4CzIPN:BPEB and $\tau_T = 63$ μs for 4CzIPN:BPEB(OC_8H_{17})$_2$. Therefore, the similar triplet lifetime values yield comparable threshold

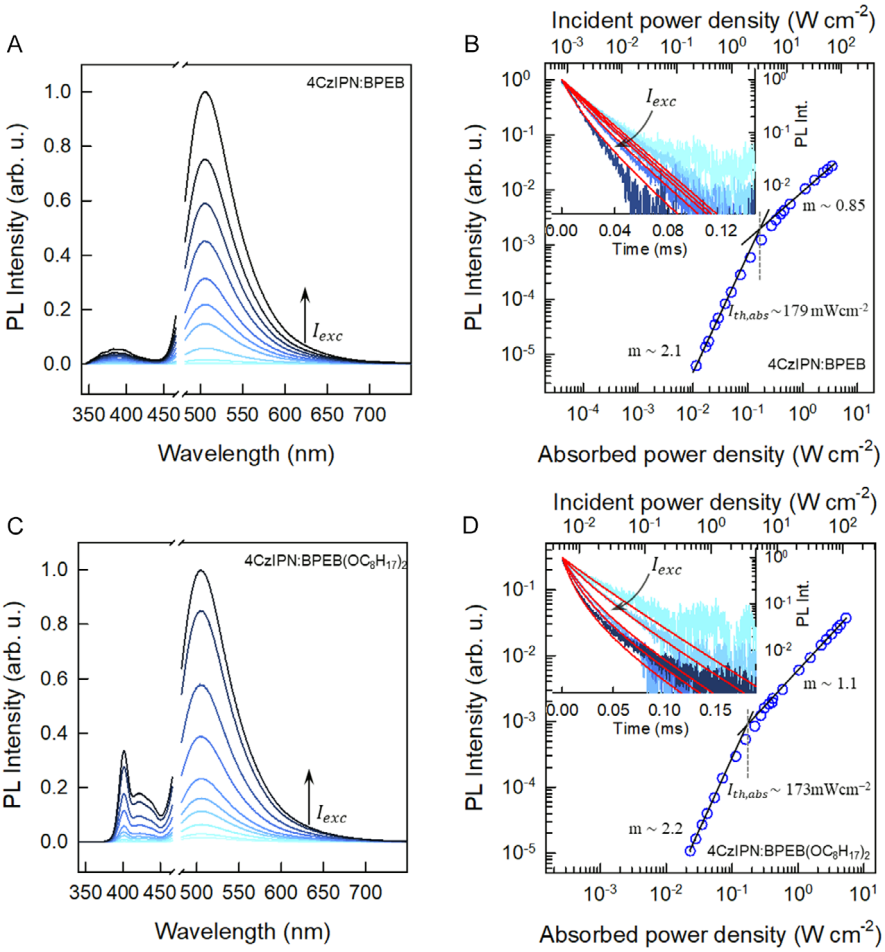

FIGURE 5 | (A,C) Spectra showing the upconverted emission of degassed solutions of 4CzIPN paired with BPEB and BPEB(OC_8H_{17})$_2$ in toluene (c 4CzIPN = 5×10^{-4} M; c emitters = 5×10^{-3} M) under cw excitation at 473 nm. The excitation intensity I_{exc} was gradually increased. Aside from the residual 4CzIPN emission band with maximum at 505 nm, the spectra show an I_{exc}-dependent increase in emission centered around 380 and 400 nm. (B,D) Double-log plots of integrated UC PL intensity versus absorbed power density for 4CzIPN:BPEB and 4CzIPN:BPEB(OC_8H_{17})$_2$ (blue circles). The solid black lines with slope given by the parameter m reported represent linear fits used to determine the intersection point corresponding to a threshold intensity of ca. 179 (B) and 173 (D) mW·cm^{-2}. The insets show time-resolved UC emission decays recorded at increasing excitation intensities (shaded traces).

intensities, according to Equation (4). Besides supporting the experimental evidence, these findings suggest a possible interaction between the 4CzIPN sensitizer and annihilators that may reduce the BPEB(OC_8H_{17})$_2$ triplet lifetime and limit the efficiency at low powers. However, despite their higher I_{th}, the 4CzIPN-based systems demonstrate superior UC efficiencies, with Φ_{UC} ca. 3.2% for BPEB and ca. 4.5% for BPEB(OC_8H_{17})$_2$. These values are significantly higher than the Φ_{UC} measured for the 4CzBN-based system, most probably due to a lower reabsorption of the UC photons with an enhanced global light output. Once again, the BPEB(OC_8H_{17})$_2$ annihilator yields a higher Φ_{UC} because of its larger statistical probability to get singlets from TTA [38]. A broader comparison across all four systems reveals complementary advantages. The 4CzBN:BPEB(OC_8H_{17})$_2$ system clearly excels in achieving UC at low excitation powers close to the solar irradiance (I_{th} ca. 25 mW·cm^{-2}), making it suitable for low-power applications. This is attributed primarily to the long-living triplets of the annihilator. On the other hand, the 4CzIPN:BPEB(OC_8H_{17})$_2$ pair achieves the highest Φ_{UC} (ca. 4.5%) under higher-intensity excitation, offering better photon economy at higher intensities. Notably, BPEB(OC_8H_{17})$_2$ performs consistently better than the parent BPEB with both sensitizers, confirming its versatility and the effectiveness of the alkoxylation in making better TTA annihilators. Overall, these results highlight the potential of combining tunable TADF sensitizers with structurally engineered emitters, also finely controlling the interplay between τ_T, Φ_{ET}, and the dynamics of TADF to achieve balanced and optimized all-organic TTA-UC systems [40, 45].

3 | Conclusion

This study demonstrates the successful implementation of TADF sensitizers and bis(phenylethynyl)benzene-based emitters in Vis-to-UV TTA-UC systems, which represent metal-free alternatives to organometallic approaches. Two well-characterized TADF compounds, 4CzBN and 4CzIPN, were paired with BPEB and its alkoxylated derivative BPEB(OC_8H_{17})$_2$, to form four distinct sensitizer–annihilator pairs. Efficient ET was observed in all cases, with transfer efficiencies up to 88% for the 4CzBN-based systems and up to 68% for those using 4CzIPN. Each pair successfully generated upconverted UV emission centered at ca. 380 or

400 nm, respectively, with excitation at 405 or 473 nm, which translates into anti-Stokes shifts of ca. 200 meV and 38 meV with 4CzBN, and ca. 642 meV and 480 meV with 4CzIPN. Notably, the 4CzBN:BPEB(OC_8H_{17})$_2$ system exhibits a remarkably low excitation threshold intensity of 25 mW·cm^{-2}, a value among the lowest reported for fully organic UV TTA-UC systems, which correlates with its longer emitter triplet lifetime and improved singlet generation efficiency. On the other hand, systems employing 4CzIPN showed higher threshold intensities but one order of magnitude higher UC efficiency reaching about 5% yield in the generation of UV photons, an excellent value considering the embryonal state of the TTA-UC system based on TADF triplet sensitizers. Together, these findings confirm that TADF sensitizers are viable and sustainable alternatives to heavy-metal complexes in TTA-UC systems, with structure and properties that can be potentially exploited to fine-tune UC performance. The combination of TADF dyes and BPEB-based emitters offers a fully organic platform for future low-power UV-emitting technologies, including solar-driven photochemistry and photonic applications.

4 | Experimental Section

4.1 | Materials

Unless otherwise specified, all chemicals used in the experiments were obtained from commercial suppliers and employed without any further purification. These included: 2,3,5,6-tetrakis(carbazol-9-yl)benzonitrile (4CzBN, 99%, Ossila); 2,4,5,6-tetrakis(9H-carbazol-9-yl) isophthalonitrile (4CzIPN, 98%, Fluorochem); 1,4-bis(phenylethynyl)benzene (BPEB, 97%, Fluorochem); toluene (99.8%, Fisher Chemical and Sigma–Aldrich); tetrahydrofuran (99.9%, Sigma–Aldrich). The compound 1,4-bis((4-(octyloxy) phenyl)ethynyl)benzene (BPEB(OC_8H_{17})$_2$) was synthesized as reported before [37].

4.2 | Sample Preparation

All samples were dissolved in toluene and transferred into quartz cuvettes with a 0.1 cm optical path length for optical measurements. For energy transfer and UC experiments, samples were handled inside a nitrogen-filled glove box (oxygen level maintained below 1 ppm) to minimize quenching of triplet states by molecular oxygen. Once prepared, the samples were hermetically sealed to prevent oxygen contamination [46].

4.3 | Photophysical Studies

Optical absorption spectra were acquired under normal incidence using an Agilent Cary 60 spectrometer and 1 mm-thick quartz cuvettes. Steady-state PL measurements at room temperature were performed with a Varian Cary Eclipse fluorescence spectrometer. Excitation was achieved using emission from the integrated Xe lamp, and detection of the emitted signal was carried out using a phototube. All spectra were corrected to account for the instrument's spectral response.

Steady-state UC PL spectra were recorded using a continuous-wave diode-pumped solid-state (DPSSL) laser emitting at 473 nm (MBL-III-473-10 mW) for measurements based on 4CzIPN and at 405 nm (RLTMDL-405-50-3) for those based on 4CzBN, both lasers equipped with TTL modulation. The emission spectra were collected via a charge-coupled device (CCD) detector (Jobin-Yvon Syncerity) interfaced with a Jobin-Yvon Triax 190 monochromator fitted with a 300 lines/mm grating. While the reported spectra were left uncorrected for spectral response (to minimize noise at the blue edge), response-corrected spectra were used for the calculation of UC efficiencies. The excitation intensity was modulated using reflective neutral density filters between the laser and the sample, and the power density incident on the sample was measured using a Thorlabs PM100USB optical power meter in combination with an S120VC sensor head. The beam diameter was determined using the knife-edge technique.

Time-resolved UC measurements as a function of excitation power were carried out using the same 473 nm or 405 nm cw lasers, modulated via a square wave signal (500 Hz) generated by a TTi TG5011 waveform generator. The resulting signal was detected with a nitrogen-cooled photomultiplier tube (Hamamatsu R5509−73), amplified using a Hamamatsu C5594 high-speed amplifier, and processed through a 74 100 Cornerstone 260 ¼ m VIS-NIR monochromator (ORIEL) coupled with a PCI plug-in ORTEC 9353 time digitizer/multichannel scaler operating in TCSPC mode (temporal resolution ≈ 400 ps).

For time-resolved energy transfer experiments, a 405 nm picosecond-pulsed diode laser (Edinburgh EPL405) was used as excitation source, with detection performed on a FLS980 spectrometer (Edinburgh Instruments) coupled with a PicoQuant PMA Hybrid Series-07 and a PicoHarp 300 time-correlated single photon counting unit.

The time-resolved data of the 4CzBN and 4CzIPN PL at low temperature were acquired using a digital oscilloscope (TDS 1001C-EDU), under the same excitation source.

4.4 | PL Quantum Yield

The PL quantum yields Φ_F of the studied molecules were determined by comparing their emission spectra with that of a reference compound of known quantum yield Φ_{ref}, following Equation (5):

$$\Phi_F = \Phi_{ref} \frac{I_s}{I_{ref}} \frac{A_{ref}}{A_s} \frac{n_s^2}{n_{ref}^2} \quad (5)$$

In Equation (5), I represents the PL intensity of either the sample (s) or reference (ref), A is the fraction of light absorbed at the excitation wavelength, and n corresponds to the refractive index of the solvents used. All comparative measurements were conducted under identical experimental conditions to ensure accuracy and consistency.

To assess the quantum yield of the emitters, a solution ($c = 3.7 \times 10^{-5}$ M) of 2,5-diphenyloxazole (PPO, $\Phi_{ref} = 1$) in cyclohexane was used as the standard [47]. For determining the Φ_{PL} of the TADF sensitizers at the concentrations employed in the UC experiments, a 9,10-diphenylanthracene (DPA) solution ($c = 1 \times 10^{-4}$ M) in cyclohexane (DPA, $\Phi_{ref} = 0.97$) [48] was used as the reference. The measured fluorescence quantum yield Φ_{sens} of 4CzBN and 4CzIPN are 0.43 and 0.97.

4.5 | UC Quantum Yield

Due to the difficulty in identifying a suitable standard for a direct determination of the UC quantum yield Φ_{UC}, we estimated its value by analyzing the ratio of upconverted emission to residual sensitizer emission (I_{UC} and I_{sens}, respectively) within the excitation intensity range where I_{UC} displays linear dependence. Considering that the energy transfer process affects only the delayed emission, the Φ_{UC} values were calculated according to Equation (6):

$$\Phi_{UC} = \left(\Phi_{prompt} + \Phi_{delayed}(1 - \Phi_{ET})\right)\frac{I_{UC}}{I_{sens}} \quad (6)$$

The Φ_{prompt} values of 4CzBN (0.11) and 4CzIPN (0.15) were taken from Refs. [21, 35, 49] and the corresponding $\Phi_{delayed}$ values were calculated as $\Phi_{sens} - \Phi_{prompt}$. When using 4CzBN as sensitizer, the Φ_{ET} values calculated from time-resolved measurements were considered.

Author Contributions

Davide Lardani: conceptualization (supporting), data curation (lead), formal analysis (supporting), investigation (lead), methodology (supporting), writing – original draft (lead), and writing – review and editing (equal). **Alessandra Ronchi**: data curation (equal), formal analysis (lead), investigation (lead), methodology (lead), writing – original draft (lead), and writing – review and editing (equal). **Xueqian Hu**: investigation (supporting), methodology (supporting), writing – original draft (supporting), and writing – review and editing (supporting). **Angelo Monguzzi**: conceptualization (lead), formal analysis (lead), funding acquisition (lead), methodology (supporting), project administration (lead), resources (lead), supervision (lead), writing – original draft (supporting), and writing – review and editing (supporting). **Christoph Weder**: conceptualization (equal), formal analysis (supporting), funding acquisition (lead), project administration (lead), resources (lead), supervision (lead), writing – original draft (supporting), and writing – review and editing (equal).

Acknowledgements

The authors gratefully acknowledge financial support from the Swiss National Science Foundation (SNSF, grant no. 200020-197209) and the Adolphe Merkle Foundation. AM and AR also recognize funding from the National Plan for NRRP Complementary Investments (PNC), project n. PNC0000003 – AdvaNced Technologies for Human-centrEd Medicine (ANTHEM). Additional support to AR was provided by the Italian Ministry of Research through the PRIN2022 program (project Luminance, 2022E42PMA), funded by the European Union - Next Generation EU initiative.

Open access publishing facilitated by Universite de Fribourg, as part of the Wiley - Universite de Fribourg agreement via the Consortium Of Swiss Academic Libraries.

Funding

This work was supported by the Swiss National Science Foundation (SNSF) (200020-197209), the Adolphe Merkle Foundation, the National Plan for NRRP Complementary Investments (PNC), (PNC0000003), AdvaNced Technologies for Human-centrEd Medicine (ANTHEM), and the Italian Ministry of Research (PRIN2022), (2022E42PMA), the European Union – Next Generation EU.

Conflicts of Interest

The authors declare no conflicts of interest.

Data Availability Statement

The dataset underlying the findings of this article can be found at https://doi.org/10.5281/zenodo.17119988.

References

1. P. Venkatesan, J. Y. Lin, D. Roy, P. Aloni, Z. F. Lin, and R. A. Doong, "Enhanced Solar-Driven Photoelectrocatalytic Water Treatment and Hydrogen Evolution with Triplet-Triplet Annihilation Upconversion with Mo-Doped $BiVO_4$ Nanocomposite Films," *Applied Catalysis B: Environmental* 365 (2025): 124913, https://doi.org/10.1016/j.apcatb.2024.124913.

2. D. K. Limberg, J. H. Kang, and R. C. Hayward, "Triplet–Triplet Annihilation Photopolymerization for High-Resolution 3D Printing," *Journal of the American Chemical Society* 144 (2022): 5226–5232, https://doi.org/10.1021/jacs.1c11022.

3. C. J. O'Dea, J. Isokuortti, E. E. Comer, S. T. Roberts, and Z. A. Page, "Triplet Upconversion under Ambient Conditions Enables Digital Light Processing 3D Printing," *ACS Central Science* 10 (2024): 272–282, https://doi.org/10.1021/acscentsci.3c01263.

4. C. Kerzig and O. S. Wenger, "Sensitized Triplet–triplet Annihilation Upconversion in Water and Its Application to Photochemical Transformations," *Chemical Science* 9 (2018): 6670–6678, https://doi.org/10.1039/C8SC01829D.

5. B. S. Richards, D. Hudry, D. Busko, A. Turshatov, and I. A. Howard, "Photon Upconversion for Photovoltaics and Photocatalysis: A Critical Review," *Chemical Reviews* 121, no. 15 (2021): 9165–9195, https://doi.org/10.1021/acs.chemrev.1c00034.

6. S. S. Saric-Bosanac, A. K. Clark, V. Nguyen, et al., "Quantification of Ultraviolet (UV) Radiation in the Shade and in Direct Sunlight," *Dermatology Online Journal* (2019): 25, https://doi.org/10.5070/D3257044801.

7. Y. Wei, K. Pan, X. Cao, Y. Li, X. Zhou, and C. Yang, "Multiple Resonance Thermally Activated Delayed Fluorescence Sensitizers Enable Green-to-Ultraviolet Photon Upconversion: Application in Photochemical Transformations," *CCS Chemistry* 4 (2022): 3852–3863, https://doi.org/10.31635/ccschem.022.202101507.

8. Y. Murakami, A. Motooka, R. Enomoto, K. Niimi, A. Kaiho, and N. Kiyoyanagi, "Visible-to-Ultraviolet (<340 Nm) Photon Upconversion by Triplet–triplet Annihilation in Solvents," *Physical Chemistry Chemical Physics* 22 (2020): 27134–27143, https://doi.org/10.1039/D0CP04923A.

9. M. Uji, T. J. B. Zähringer, C. Kerzig, and N. Yanai, "Visible-to-UV Photon Upconversion: Recent Progress in New Materials and Applications," *Angewandte Chemie International Edition* 62, no. 25 (2023): 1–22, https://doi.org/10.1002/anie.202301506.

10. A. J. Carrod, V. Gray, and K. Börjesson, "Recent Advances in Triplet–triplet Annihilation Upconversion and Singlet Fission, towards Solar Energy Applications," *Energy & Environmental Science* 15 (2022): 4982–5016, https://doi.org/10.1039/D2EE01600A.

11. Y. C. Simon and C. Weder, "Low-Power Photon Upconversion through Triplet–triplet Annihilation in Polymers," *Journal of Materials Chemistry* 22 (2012): 20817–20830, https://doi.org/10.1039/C2JM33654E.

12. F. Edhborg, A. Olesund, and B. Albinsson, "Best Practice in Determining Key Photophysical Parameters in Triplet–triplet Annihilation Photon Upconversion," *Photochemical & Photobiological Sciences* 21 (2022): 1143–1158, https://doi.org/10.1007/s43630-022-00219-x.

13. D. Jefferies, T. W. Schmidt, and L. Frazer, "Photochemical Upconversion Theory: Importance of Triplet Energy Levels and Triplet Quenching," *Physical Review Applied* 12 (2019): 024023, https://doi.org/10.1103/PhysRevApplied.12.024023.

14. T. N. Singh-Rachford and F. N. Castellano, "Photon Upconversion Based on Sensitized Triplet–triplet Annihilation," *Coordination*

Chemistry Reviews 254 (2010): 2560–2573, https://doi.org/10.1016/j.ccr.2010.01.003.

15. I. S. Alkhaibari, X. Zhang, J. Zhao, et al., "Tuning Excited State Character in Iridium(III) Photosensitizers and Its Influence on TTA-UC," *Inorganic Chemistry* 63, no. 21 (2024): 9931–9940, https://doi.org/10.1021/acs.inorgchem.4c01003.

16. V. Gray, K. Moth-Poulsen, B. Albinsson, and M. Abrahamsson, "Towards Efficient Solid-State Triplet–triplet Annihilation Based Photon Upconversion: Supramolecular, Macromolecular and Self-Assembled Systems," *Coordination Chemistry Reviews* 362 (2018): 54–71, https://doi.org/10.1016/j.ccr.2018.02.011.

17. P. Jin and C. Wang, "Photon Upconversion Sensitized by Earth-Abundant Transition Metal Complexes," *Physical Chemistry Chemical Physics* 27 (2025): 13793–13811, https://doi.org/10.1039/D5CP00333D.

18. E. U. Mughal, N. Naeem, S. F. Kainat, et al., "Advances in the Design of Thermally Activated Delayed Fluorescence Materials for High-Efficiency OLEDs," *Journal of Photochemistry and Photobiology C: Photochemistry Reviews* 64 (2025): 100700, https://doi.org/10.1016/j.jphotochemrev.2025.100700.

19. E. U. Mughal, S. F. Kainat, A. M. Almohyawi, et al., "Thermally Activated Delayed Fluorescence Materials: Innovative Design and Advanced Application in Biomedicine, Catalysis and Electronics," *RSC Advances* 15 (2025): 7383–7471, https://doi.org/10.1039/D5RA00157A.

20. J. M. Dos Santos, D. Hall, B. Basumatary, et al., "The Golden Age of Thermally Activated Delayed Fluorescence Materials: Design and Exploitation," *Chemical Reviews* 124, no. 24 (2024): 13736–14110, https://doi.org/10.1021/acs.chemrev.3c00755.

21. H. Uoyama, K. Goushi, K. Shizu, H. Nomura, and C. Adachi, "Highly Efficient Organic Light-Emitting Diodes from Delayed Fluorescence," *Nature* 492 (2012): 234–238, https://doi.org/10.1038/nature11687.

22. R. Keruckiene, A. A. Vaitusionak, M. I. Hulnik, et al., "Is a Small Singlet–triplet Energy Gap a Guarantee of TADF Performance in MR-TADF Compounds? Impact of the Triplet Manifold Energy Splitting," *Journal of Materials Chemistry C* 12 (2024): 3450–3464, https://doi.org/10.1039/D3TC04397E.

23. J. Eng and T. J. Penfold, "Open Questions on the Photophysics of Thermally Activated Delayed Fluorescence," *Communications Chemistry* 4 (2021): 21–24, https://doi.org/10.1038/s42004-021-00533-y.

24. M. Zheng, Y. Li, Y. Wei, L. Chen, S. Liu, and X. Zhou, "Highly Efficient Triplet–Triplet Annihilation Upconversion with a Thermally Activated Delayed Fluorescence Molecule as Triplet Photosensitizer," *The Journal of Physical Chemistry C* 127, no. 6 (2023): 2846–2854, https://doi.org/10.1021/acs.jpcc.2c07906.

25. B. Yurash, A. Dixon, C. Espinoza, et al., "Efficiency of Thermally Activated Delayed Fluorescence Sensitized Triplet Upconversion Doubled in Three-Component System," *Advanced Materials* 34 (2022): 2103976, https://doi.org/10.1002/adma.202103976.

26. Y. Tian, Y. Z. Shi, X. C. Fan, et al., "Exploring the Key Factors of TADF Materials as Sensitizers: Toward High-Performance Triplet Fusion Upconversion," *Advanced Optical Materials* 11 (2023): 2300504, https://doi.org/10.1002/adom.202300504.

27. Q. Chen, Y. Liu, X. Guo, et al., "Energy Transfer Dynamics in Triplet–Triplet Annihilation Upconversion Using a Bichromophoric Heavy-Atom-Free Sensitizer," *The Journal of Physical Chemistry A* 122, no. 33 (2018): 6673–6682, https://doi.org/10.1021/acs.jpca.8b05901.

28. M. Hussain, S. S. Razi, T. Tao, and F. Hartl, "Triplet-Triplet Annihilation Photon up-Conversion: Accessing Triplet Excited States with Minimum Energy Loss," *Journal of Photochemistry and Photobiology C: Photochemistry Reviews* 56 (2023): 100618, https://doi.org/10.1016/j.jphotochemrev.2023.100618.

29. N. Yanai and N. Kimizuka, "New Triplet Sensitization Routes for Photon Upconversion: Thermally Activated Delayed Fluorescence Molecules, Inorganic Nanocrystals, and Singlet-to-Triplet Absorption," *Accounts of Chemical Research* 50, no. 10 (2017): 2487–2495, https://doi.org/10.1021/acs.accounts.7b00235.

30. N. Yanai, M. Kozue, S. Amemori, R. Kabe, C. Adachi, and N. Kimizuka, "Increased Vis-to-UV Upconversion Performance by Energy Level Matching between a TADF Donor and High Triplet Energy Acceptors," *Journal of Materials Chemistry C* 4 (2016): 6447–6451, https://doi.org/10.1039/C6TC01816E.

31. J. Peng, X. Guo, X. Jiang, D. Zhao, and Y. Ma, "Developing Efficient Heavy-Atom-Free Photosensitizers Applicable to TTA Upconversion in Polymer Films," *Chemical Science* 7 (2016): 1233–1237, https://doi.org/10.1039/C5SC03245H.

32. T. C. Wu, D. N. Congreve, and M. A. Baldo, "Solid State Photon Upconversion Utilizing Thermally Activated Delayed Fluorescence Molecules as Triplet Sensitizer," *Applied Physics Letters* 107 (2015): 031103, https://doi.org/10.1063/1.4926914.

33. D. Han, X. Yang, J. Han, J. Zhou, T. Jiao, and P. Duan, "Sequentially Amplified Circularly Polarized Ultraviolet Luminescence for Enantioselective Photopolymerization," *Nature Communications* 11 (2020): 5659, https://doi.org/10.1038/s41467-020-19479-1.

34. T. J. B. Zähringer, M. S. Bertrams, and C. Kerzig, "Purely Organic Vis-to-UV Upconversion with an Excited Annihilator Singlet beyond 4 eV," *Journal of Materials Chemistry C* 10 (2022): 4568–4573, https://doi.org/10.1039/D1TC04782E.

35. A. Olesund, J. Johnsson, F. Edhborg, S. Ghasemi, K. Moth-Poulsen, and B. Albinsson, "Approaching the Spin-Statistical Limit in Visible-to-Ultraviolet Photon Upconversion," *Journal of the American Chemical Society* 144, no. 8 (2022): 3706–3716, https://doi.org/10.1021/jacs.1c13222.

36. H. L. Lee, M. S. Lee, H. Park, W. S. Han, and J. H. Kim, "Visible-to-UV Triplet-Triplet Annihilation Upconversion from a Thermally Activated Delayed Fluorescence/Pyrene Pair in an Air-Saturated Solution," *Korean Journal of Chemical Engineering* 36 (2019): 1791–1798, https://doi.org/10.1007/s11814-019-0355-2.

37. A. R. A. Palmans, M. Eglin, A. Montali, C. Weder, and P. Smith, "Tensile Orientation Behavior of Alkoxy-Substituted Bis(phenylethynyl)benzene Derivatives in Polyolefin Blend Films," *Chemistry of Materials* 12 (2000): 472–480, https://doi.org/10.1021/cm990558.

38. D. Lardani, A. Ronchi, X. Hu, A. Monguzzi, and C. Weder, "Bis(phenylethynyl)benzenes Enable Stable Visible-to-Ultraviolet Sensitized Triplet–triplet Annihilation Upconversion," *Journal of Materials Chemistry C* 13 (2025): 18796–18804, https://doi.org/10.1039/D5TC02434J.

39. A. Monguzzi, R. Tubino, S. Hoseinkhani, M. Campione, and F. Meinardi, "Low Power, Non-Coherent Sensitized Photon up-Conversion: Modelling and Perspectives," *Physical Chemistry Chemical Physics* 14 (2012): 4322–4332, https://doi.org/10.1039/C2CP23900K.

40. T. Hosokai, H. Matsuzaki, H. Nakanotani, et al., "Evidence and Mechanism of Efficient Thermally Activated Delayed Fluorescence Promoted by Delocalized Excited States," *Science Advances* 3 (2017): e1603282, https://doi.org/10.1126/sciadv.1603282.

41. X. Zhou, J. Nikan, K. Guo, P. W. M. Blom, G. J. A. H. Wetzelaer, and Y. Li, "Determination of the Kinetic Rates and Intrinsic Nonradiative Losses in Organic Thermally Activated Delayed Fluorescence Emitters," *Advanced Science* 12 (2025): 05338, https://doi.org/10.1002/advs.202505338.

42. A. Monguzzi, J. Mézyk, F. Scotognella, R. Tubino, and F. Meinardi, "Upconversion-Induced Fluorescence in Multicomponent Systems: Steady-State Excitation Power Threshold," *Physical Review B* 78 (2008): 195112, https://doi.org/10.1103/PhysRevB.78.195112.

43. S. M. Bachilo and R. B. Weisman, "Determination of Triplet Quantum Yields from Triplet−Triplet Annihilation Fluorescence," *The Journal of*

Physical Chemistry A 104, no. 33 (2000): 7711–7714, https://doi.org/10.1021/jp001877n.

44. T. W. Schmidt and F. N. Castellano, "Photochemical Upconversion: The Primacy of Kinetics," *The Journal of Physical Chemistry Letters* 5, no. 22 (2014): 4062–4072, https://doi.org/10.1021/jz501799m.

45. Y. Olivier, B. Yurash, L. Muccioli, et al., "Nature of the Singlet and Triplet Excitations Mediating Thermally Activated Delayed Fluorescence," *Physical Review Materials* 1 (2017): 075602, https://doi.org/10.1103/PhysRevMaterials.1.075602.

46. K. Kawaoka, A. U. Khan, and D. R. Kearns, "Role of Singlet Excited States of Molecular Oxygen in the Quenching of Organic Triplet States," *The Journal of Chemical Physics* 46 (1967): 1842–1853, https://doi.org/10.1063/1.1840943.

47. I. B. Berlman, *Handbook of Fluorescence Spectra of Aromatic Molecules*, Academic Press, Academic Press, (1971).

48. K. Suzuki, A. Kobayashi, S. Kaneko, et al., "Re-Evaluation of Absolute Luminescence Quantum Yields of Standard Solutions Using a Spectrometer with an Integrating Sphere and a Back-Thinned CCD Detector," *Physical Chemistry Chemical Physics* 11 (2009): 9850–9860, https://doi.org/10.1039/B912178A.

49. H. Noda, X. K. Chen, H. Nakanotani, et al., "Critical Role of Intermediate Electronic States for Spin-Flip Processes in Charge-Transfer-Type Organic Molecules with Multiple Donors and Acceptors," *Nature Materials* 18 (2019): 1084–1090, https://doi.org/10.1038/s41563-019-0465-6.

Supporting Information

Additional supporting information can be found online in the Supporting Information section. **Supporting Fig. S1:** (A) Absorption (black line) and photoluminescence (PL) spectra of a degassed 4CzBN solution in toluene ($c = 5 \times 10^{-4}$ M). The PL spectra were recorded at 300 K (red line) and 77 K (blue line). (B) Time-resolved PL decay of the same solution measured at 77 K under 405 nm modulated laser excitation, showing phosphorescence from the T_1 state. The fitted decay (black line) yields a triplet lifetime of $\tau_T = 165$ ms. (C) Time-resolved PL decay of the same solution at 300 K under 405 nm pulsed laser excitation. The graph displays the PL intensity, i.e., delayed fluorescence resulting from reverse intersystem crossing, as a function of time. The process has a lifetime of $\tau_{delayed} = 25.3$ µs. The inset shows the prompt fluorescence component with a lifetime of $\tau_{prompt} = 1.58$ ns. **Supporting Fig. S2:** Time-resolved PL decay of 4CzBN in the absence (dark red) and presence of BPEB (red) or BPEB(OC_8H_{17})$_2$ (orange) in degassed toluene ($c = 5 \times 10^{-4}$ M for 4CzBN and $c = 5 \times 10^{-3}$ M for BPEB and BPEB(OC_8H_{17})$_2$), acquired at 450 nm under pulsed excitation at 405 nm. The green lines are the fitting curves according to bi-exponential functions to estimate the lifetime of the prompt and delayed emissions. The results of the fitting procedure are reported in Table S1. **Supporting Fig. S3:** (A) Absorption and PL spectra of 4CzIPN ($c = 5 \times 10^{-4}$ M in degassed toluene). The red curve shows the PL spectrum at room temperature (300 K), while the blue curve corresponds to the PL recorded at 77 K. (B) Time-resolved PL decay measured at 77 K under 405 nm modulated laser excitation, showing phosphorescence from the T_1 state. The fitted decay (black line) yields a triplet lifetime of $\tau_T = 204$ ms. (C) Time-resolved PL decay at 300 K under 405 nm pulsed laser excitation. The main panel shows delayed fluorescence from rISC, while the inset displays the prompt fluorescence component. **Supporting Fig. S4:** Time-resolved PL decay of 4CzIPN in the absence (dark red) and presence of BPEB (red) or BPEB(OC_8H_{17})$_2$ (orange) in degassed toluene ($c = 5 \times 10^{-4}$ M for 4CzBN and $c = 5 \times 10^{-3}$ M for BPEB and BPEB(OC_8H_{17})$_2$), acquired at 505 nm under pulsed excitation at 405 nm. The green lines are the fitting curves according to bi-exponential functions. The results of the fitting procedure are reported in Table S2. **Supporting Fig. S5:** (A B) Concentration-dependent sensitizer-to-annihilator energy transfer yield Φ_{ET} measured in degassed toluene solutions. The symbols mark the experimental Φ_{ET} values measured for solutions of (A) 4CzBN ($c = 5\times10^{-4}$ M) or (B) 4CzIPN ($c = 5\times10^{-4}$ M) mixed with BPEB or BPEB(OC_8H_{17})$_2$ at four different concentrations ($c = 5\times10^{-3}$ M, 2.5×10^{-3} M, 1×10^{-3} M and 5×10^{-4} M). Dashed and solid black lines are fits of the data with the Φ_{ET} values predicted considering the process in the rapid diffusion regime through Eq. S1 and S2. The fit curves allow the estimation of characteristic energy transfer rate constants of 4.27×10^{-13} cm^3 s^{-1} for the 4CzBN and BPEB or BPEB(OC_8H_{17})$_2$ and 5.49×10^{-13} cm^3 s^{-1} for 4CzIPN and BPEB or BPEB(OC_8H_{17})$_2$. **Supporting Table S1:** Results of the fitting procedure of the experimental data reported in Figure S2, according to bi-exponential functions for the systems based on 4CzBN. **Supporting Table S2:** Results of the fitting procedure of the experimental data reported in Figure S4, according to bi-exponential functions for the systems based on 4CzIPN. **Supporting Table S3:** Parameters employed to model the ET in the rapid diffusion regime approximation.